Chapter 8

Light Emitters

Silicon is a classic example of an indirect semiconductor (see Chapter 2). The indirect bandgap E_{gind} is created by a transition between band states (valence band edge) of zero wave number (k = 0), conventionally called the Γ point, and the lowest lying conduction band states at a high wave number ($k > 0$), called the Δ point. The Δ point is situated on the x axis (and on the equivalent y and z axes) near the end of this axis within the first Brillouin zone. This endpoint is called the X point. The corresponding wave number k_x is given by (diamond lattice)

$$k_x = 2\pi/a. \tag{8.1}$$

The Δ point in Si is roughly given by

$$k_\Delta = 4/5k_x. \tag{8.2}$$

Transitions of carriers across the indirect bandgap need an energy transfer of E_{gind} and a momentum transfer of $\hbar k_\Delta$. The energy transfer is easily provided by a photon, whereas the large momentum transfer k_Δ needs the help of a phonon, which reduces the radiation transition probability of the indirect semiconductor. The wave number of the photon k_{phot} is rather small (about a factor 10^{-4}) compared to the Brillouin zone edge.

$$k_{\text{phot}} = {}^{q}\!/_{\hbar c} V_{\text{gind}} \tag{8.3}$$

Silicon-Based Photonics
Erich Kasper and Jinzhong Yu

ISBN 978-981-4303-24-8 (Hardcover), 978-1-315-15651-4 (eBook)
www.jennystanford.com

The energy of the photon is usually measured by the corresponding voltage V_{gind} (this energy unit is called eV)

$$E_{\text{gind}} = qV_{\text{gind}} \tag{8.4}$$

The proportionality factor $q/\hbar c$ is equal to $5.06.10^6$/Vm. This means that a photon with around 1 eV energy has a negligible wave number compared to the wave number (about 10^{11}/m) of the Brillouin zone edge. Phonons have low energies (typically tens of millielectron volts), and they span in terms of wave number the full range of the Brillouin zone (for more details, see Chapter 2). Usually, photoluminescence (PL) from Si shows weak emission lines of energies below the bandgap (photon replica). The most significant contribution [1] stems from the transverse optical (TO) phonon, with energy of about 60 meV. Nevertheless, good radiative quantum efficiencies of about 10% may be obtained with very pure bulk Si and low injection levels. Then competitive nonradiative recombination channels (recombination from impurities and Auger recombination are weakly addressed) are also weak. Large emission volumes and low emission intensities prohibit usage in a device structure. The direct transition is much higher in energy than the indirect one. The lowest (Γ) point energy in a Si conduction band is more than 2 eV above the indirect (Δ) minimum. This energy difference for SiGe decreases but is always too high for a meaningful electron occupation probability except for pure Ge or GeSn.

Emission across the bandgap is the favored solution for semiconductor materials but not the only possibility. Let us consider two different paths of light generation without recombination across the bandgap. One is based on the incorporation of atoms with individual atomic emission properties, and the other relies on a nonequilibrium carrier distribution within the bands.

Rare earth elements have distinct energy level transitions that cover the full spectrum between near infrared and ultraviolet. The rare earth elements can be easily incorporated in glass. The optical stimulation of the emission is effective; also the electrical stimulation delivers good quantum efficiencies (10% and more), but the power efficiency [2] suffers from the high voltages (typically 100 V) needed to inject electrons into a thin glass layer. In semiconductors, the incorporation of rare earth elements is more difficult, resulting in rather low concentrations or poor crystal quality. This technique

may be interesting for future photonic systems with integrated display functions.

A different mechanism of light emission gets active under strong electric fields easily realized in reverse-biased junctions. Electrons or holes are accelerated to get higher energies than under room temperature equilibrium. These carriers are accordingly called hot electrons (holes). Recombination of hot electrons with hot holes results in light emission [3] with energies larger than the bandgap energy. Finally, the hot carriers obtain energies (about 1.5 eV, or 40 times the equilibrium kinetic energy of an electron) to ionize neutral Si. Visible light with a broad spectral distribution is emitted from a junction biased toward avalanche breakdown, but breakdown is not a favorable mode of operation for a diode. Emission is more easily controlled with junctions that contain defects like dislocations. These junctions show a premature breakdown increase in current below the general breakdown voltage, which allows a safer operation. Defect engineering by thin, lattice mismatched SiGe layers yields diode structures with defined premature breakdown characteristics. This technique seems attractive for integration with standard complementary metal-oxide-semiconductor circuitry, and it could be used for a photonic monitoring system of safe operation of integrated circuits [4].

8.1 Bandgap Emission Mechanisms

First, we look at an ideal semiconductor with perfect periodicity. Then, we investigate the influence of structural modifications (superlattice periodicity; localization by porous Si and quantum dots) on the emission of indirect semiconductors.

8.1.1 Indirect Semiconductor Transitions

The principal structure of the bands of an indirect semiconductor is shown in Fig. 8.1. Carriers are injected, either optically or electrically, so that the band edges are populated with holes and electrons. We assume in the following that the quasi-Fermi energy levels F_p and F_n are within the bandgap. This allows approximating the carrier distributions within the band by the exponential Boltzmann

equations. It is clear that the full Fermi–Dirac statistics have to be used for high injection when the quasi-Fermi levels lie within the bands, and we will mention this if necessary. The low-energy indirect bandgap is between the conduction band edge E_c and the valence band edge E_v (Fig. 8.1).

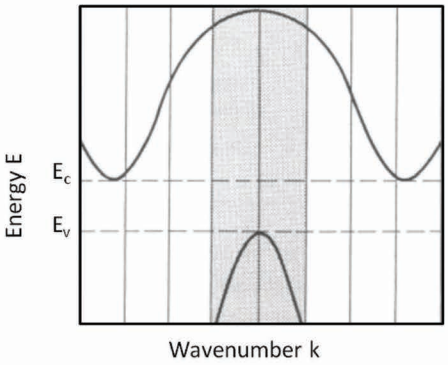

Figure 8.1 Schematic energy E diagrams versus wave number k of an indirect semiconductor (Si type with conduction band minimum at the Δ point in the k_x direction). The indirect bandgap E_{gind} is defined between the band edges E_c and E_v.

The main energy is released by a photon with energy $(E_g - E_{photon})$, where E_g is the bandgap energy and E_{photon} is the smaller phonon energy. The bandgap energy E_g measured by the light emission in slightly reduced by the excitation binding energy (excitonic bandgap). The exciton is a hole-electron pair that has to be created before a recombination process takes place. The exciton binding energy is rather small (Si: 10 meV; Ge: 3 meV). In doped material, the excitation is influenced by the charged dopant ions (bound exciton compared to free exciton in undoped material). These fine details can only be seen in low-temperature luminescence measurements. These details are overseen at higher temperatures (e.g., room temperature) by line brooding and by line shift (about $1/2k_BT$) from occupation statistics. Additionally, a weaker twin line at E_g + E_{photon} appears that is caused by the capture of a phonon existing in the material at a higher temperature. The direct transition path is represented by a vertical line in the band diagram (Fig. 8.1) because of the negligible wave number contribution of phonons. The intensity is negligible in Si and SiGe but competes with the indirect path in Ge and GeSn, as explained in the following sections.

8.1.2 Brillouin Zone Folding from the Superlattice

The band structure of a semiconductor may be modified by an overlaid periodic potential that is realized by a repeated sequence of heterostructures. The basic idea dates back to the 1970s [5, 6]. An intuitive description of the modification of the band structure gives the zone following concept. The additional periodicity with the superlattice period length L shrinks the first Brillouin zone to $\pm\ \pi/L$. Let the length L be an integral multiple n of the periodicity length $a/2$ of the diamond lattice. (Remark: The periodicity length in the diamond lattice is $a/2$ because the cubic diamond lattice cell contains $8 = 2^3$ atoms). The first Brillouin zone of the superlattice is smaller by a factor n as the diamond lattice parent cell. It is created from the parent cell by consecutive folding (Fig. 8.2) and a horizontal bending at the zone edge.

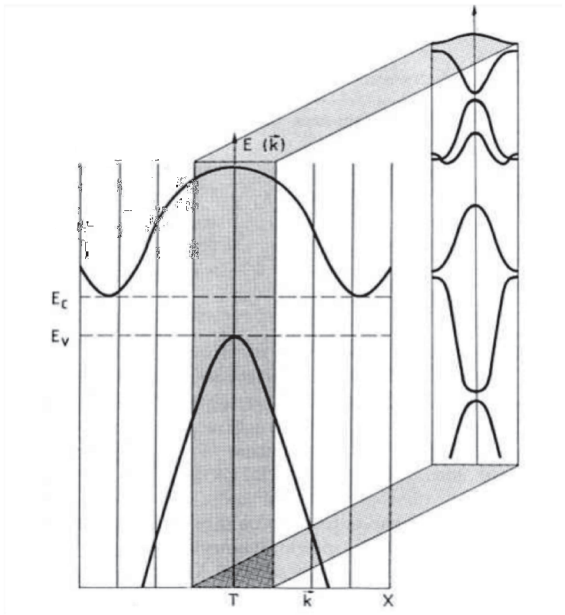

Figure 8.2 Reduction of the first Brillouin zone by a superlattice period (zone folding). Folding in four units is shown in the figure for the sake of clarity. Four minibands are created, which are separated by minigaps. The energy of the minigaps increases with a stronger superlattice potential. The essential effect for indirect semiconductors is given by the possibility to shift the position of the minimum of the conduction band with respect to the Brillouin zone edge.

By this construction, n minibands build from one parent band with small bandgaps at the zone edges. The small bandgaps at the zone edge increase with the strength of the superlattice potential. The superlattice is considered as a tailored artificial semiconductor with new electrical and optical properties. An indirect semiconductor material may change to a quasi-direct one by an appropriate choice of superlattice length [6]. First realizations with SiGe/Si superlattices started early [7], but confirmation of zone folding effects on the phonon spectra [8] and luminescence spectra [9] needed ultrathin Ge/Si superlattices with a period length L of 2.75 nm and 5.5 nm (n = 5, 10, . . .). The transition strength [10] of the quasi-direct mode is 2–3 magnitudes lower than that of a direct semiconductor.

8.1.3 Localization of Wave Functions by Quantum Structures and Porous Si

The wave numbers of states in the infinite periodic semiconductor structure are well defined. Localization of wave functions results in uncertainties of the momentum, which relaxes the need for phonon contribution to the optical transition process. This can be already seen for luminescence from the random alloy SiGe, where the statistics distribution of the Ge atoms disturbs the perfect periodicity of the diamond lattice. The PL spectrum of SiGe quantum wells [11] is already dominated by the no-phonon emission line (Fig. 8.3) from the indirect bandgap.

The Heisenberg uncertainty principle says

$$\Delta x * \Delta p_x \geq \hbar/2 \tag{8.5}$$

A stricter localization is given by a quantization in all directions—a quantum dot (QD). Two effects appear under strong quantum confinement. One effect is bandgap widening because the confined states are higher in energy than the bottom of the well or dot. The other effect is delocalization of carriers in momentum space due to the uncertainty principle, making it possible for electrons and holes to recombine directly. Nanocrystalline silicon and porous silicon behave like a large assembly of QDs. Efficient luminescence can be obtained in the visible wavelength region.

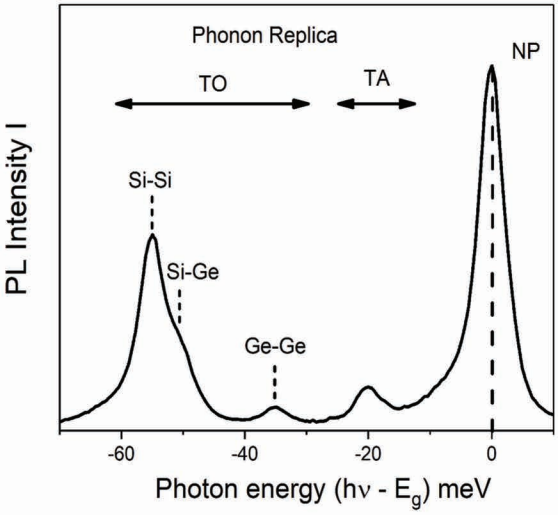

Figure 8.3 Photoluminescence intensity of SiGe layers versus photon energy ($h\nu - E_g$). The highest intensity of the random alloy provides the no-phonon peak (NP) at the excitonic bandgap. The phonon replica TO and TA (dominating in Si) are weaker and split up in three components, which can be identified as Si-Si, Si-Ge, and Ge-Ge vibrations.

8.2 Germanium Light-Emitting Diodes

For luminescence experiments, optical excitation at low temperatures is often applied (PL). For device applications, electrical excitation at room temperature is preferred (electroluminescence). The dominant electrical excitation uses diode structures for carrier injections (light-emitting diode [LED]).

8.2.1 Competition between Direct and Indirect Transitions

Ge is an indirect semiconductor like Si, but there are two essential differences: (i) the lowest lying conduction band has its minimum energy in the [111] direction at the edge of the first Brillouin zone (called the L point), and (ii) the energy difference (136 meV) between indirect and direct transition is much smaller than in Si. At room temperature, the direct bandgap is 0.80 eV and the indirect one is 0.664 eV.

The occupation probability of the direct states is much smaller than that of the indirect ones but not negligible like in Si. The direct occupation probability is about 0.4% of the indirect one within the Boltzmann approximation. Furthermore, the density of states of the direct conduction band is smaller than that of the indirect band (this is caused by the smaller effective mass of the electrons at the Γ point). Roughly, one can say that from 1000 electrons only 1 electron occupies the direct minimum; the other 999 are in the indirect minimum.

The transition probability of the direct bandgap is orders of magnitude higher than the indirect one. It is interesting to see which one is the more competitive. Early bulk Ge investigation with PL showed a strong indirect emission with a weaker direct shoulder [12]. Later investigation with epitaxial thin films [13] proved a stronger direct emission. The bulk results were explained [12] with the self-absorption of the direct line in thick substrates. The direct/indirect intensity ratio increases with temperature, favoring a room temperature operation of Ge LEDs. This observation is a consequence of the occupation statistics in indirect semiconductors, when higher temperature increases the direct/indirect occupation ratio.

A typical structure of a waveguide Ge LED is shown in Fig. 8.4 [14]. The vertical layer sequence starts with a silicon-on-insulator substrate.

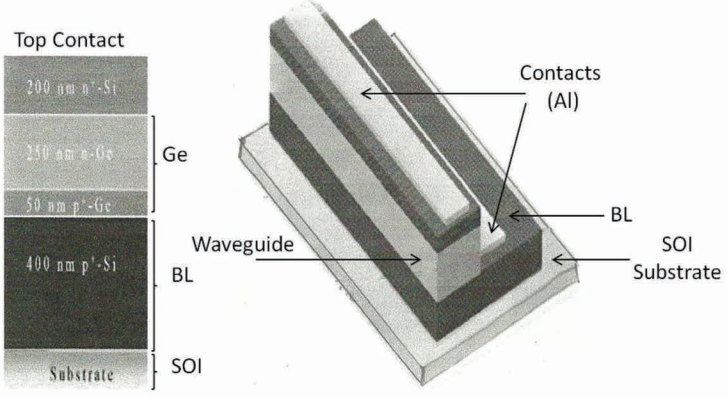

Figure 8.4 Typical layout and layer structure of a waveguide light emitter. The layer structure consists of a silicon-on-insulator (SOI) substrate with a highly p^+-doped buried layer (BL) for the backside contact. The diode junction p/n is inside the Ge waveguide. The top contact layer is n^+-Si, with Al as the top metal. Reprinted with permission from Ref. [14] © The Optical Society.

The silicon is p^+-doped to provide as the buried layer a good bottom contact property. Then follows a p^+-n Ge layer, which provides the diode structure for efficient forward current injections. The top layer is a thin n^+-Si, which provides good top contact properties and a well-behaved surface for the device technology steps.

The waveguide is structured by a dry etching step and metal contacts on the top (n-contact) and on the side (p-contact to the buried layer). The Ge LED emits light of about 1.5 µm wavelength into the waveguide when the contacts are forward biased. Interestingly, similar waveguide structures [15] can also be used for detection [16] and absorption modulation, which facilitates integration of active photonic devices.

8.2.2 Influence of Doping, Strain, and Sn Alloying

The chosen junction p^+/n is one sided and abrupt, and the junction extends to the n-side. The intensity of emission increases with the doping level at least up to an n-type doping of $3.10^{19}/cm^3$ [17]. The wavelength of emission increases by n-type doping, which is caused by the bandgap narrowing effect in highly doped semiconductors.

Another measure to increase the intensity and shift the wavelength is opened by applying tensile strain. Biaxial tensile stress [18] reduces the direct bandgap and decreases the energy difference between direct and indirect conduction band states. These effects increase the intensity and shift the wavelength. The small biaxial stress that is needed to cover the telecom bands around 1.55 µm is conventionally obtained by an annealing/cooling sequence. The tensile strain of up to 0.25% results from thermal mismatch in the expansion of the Si substrate and the Ge layer.

Alloying Ge with rather small amounts of Sn results in a reduction in the bandgap and a direct/indirect bandgap energy difference similar to the strain effect. Intensity increase and shift toward lower wavelengths are connected [19]. GeSn has a rather large lattice mismatch (14.6%) to Ge, and the equilibrium GeSn alloy is only thermodynamically stable up to rather small (<1%) Sn amounts. Metastable GeSn layers with higher amounts of Sn are grown at low temperatures [20]. Surface segregation of tin [21] and phase separation into a Ge-rich and tin-rich GeSn phase [22] limit the growth and processing conditions for device-related structures.

Stacked layers of GeSn and Ge [23] or GeSn and GeSiSn [24] are preferred multiquantum well structures for electrically stimulated LEDs. Research is ongoing to stabilize GeSiSn with high Sn amounts (>30%) on Si or Ge-on-Si platforms [25, 26].

References

1. V. Higgs, E. C. Lightowlers, G. Davies, F. Schäffler and E. Kasper (1989). Photoluminescence from MBE Si grown at low temperatures; Donor bound excitons and decorated dislocations, *Semicond. Sci. Technol.*, **4**, 593–598.
2. J. M. Sun, W. Skorupa, T. Dekorsy, M. Helm and L. Rebohle (2004). Efficient ultraviolet electroluminescence from a Gd-implanted silicon metal–oxide–semiconductor device, *Appl. Phys. Lett.*, **85**, 3387.
3. M. Morschbach, M. Oehme and E. Kasper (2007). Visible light emission by a reverse-biased integrated silicon diode, *IEEE Trans. Electron Devices*, **54**, 1091–1094.
4. E. Kasper and M. Morschbach (2013). Method for self-monitoring of breakdown in semiconductor components and semiconductor component constructed thereof, United States Patent US 8,519,732 B2.
5. L. Esaki and R. Tsu (1970). Superlattice and negative differential conductivity in semiconductors, *IBM J. Res. Dev.*, **14**, 61.
6. U. Gnutzmann and K. Clausecker (1974). Theory of direct optical transitions in an optical indirect semiconductor with a superlattice structure, *Appl. Phys.*, **3**, 9.
7. E. Kasper, H. Herzog and H. Kibbel (1975). A one-dimensional SiGe superlattice grown by UHV epitaxy, *Appl. Phys.*, **8**, 199–205.
8. H. Brugger, G. Abstreiter, H. Jorke, H. Herzog and E. Kasper (1986). Folded acoustic phonons in Si/SixGe1-x superlattices, *Phys. Rev.*, **B33**, 5928–5930.
9. R. Zachai, K. Eberl, G. Abstreiter, E. Kasper and H. Kibbel (1990). Photoluminescence in short-period Si/Ge strained layer superlattices, *Phys. Rev. Lett.*, **64**, 1055–1058.
10. G. Theodorou and E. Kasper (2007). Optical properties of Si/Ge superlattices, in *Landolt-Boernstein*, *New Series*, Vol. III, 34C3, E. Kasper and C. Klingshirn, eds. (Springer Verlag), pp. 50–86.
11. N. Usami and Y. Shiraki (2007). Single and coupled quantum wells: SiGe, in *Landolt-Boernstein*, *New Series*, Vol. III, 34C3 E. Kasper and C. Klingshirn, eds. (Springer Verlag), pp. 26–49.

12. T. Arguirov, M. Kittler, M. Oehme, N. V. Abrosimov, O. F. Vyvenko, E. Kasper and J. Schulze (2014). Luminescence from germanium and germanium on silicon, *Solid State Phenom.*, **205–206**, 383–393.

13. E. Kasper, M. Oehme, T. Arguirov, J. Werner, M. Kittler and J. Schulze (2012). Room temperature direct band gap emission from Ge p-i-n heterojunction photodiodes, *Adv. OptoElectron.*, **2012**, 916275.

14. R. Koerner, M. Oehme, M. Gollhofer, M. Schmid, K. Kostecki, S. Bechler, D. Widmann, E. Kasper and J. Schulze (2015). Electrically pumped lasing from Ge Fabry-Perot resonators on Si, *Opt. Express*, **23**, 14815–14822.

15. R. Koerner, M. Oehme, M. Gollhofer, M. Schmid, K. Kostecki, S. Bechler, D. Widmann, E. Kasper and J. Schulze (2015). Electrically pumped lasing from Ge Fabry–Perot resonators on Si, *Opt. Express*, **23**, 14815–14822.

16. A. Palmieri, M. Vallone, M. Calciati, A. Tibaldi, F. Bertazzi, G. Ghione and M. Goano (2018). Heterostructure modeling considerations for Ge-on-Si waveguide photodetectors, *Opt. Quantum Electron.*, **50**, 71.

17. M. Oehme, E. Kasper and J. Schulze (2013). GeSn heterojunction diode: detector and emitter in one device, *ECS J. Solid State Sci. Technol.*, **2**(4), 76–78.

18. M. Oehme, M. Gollhofer, D. Widmann, M. Schmid, M. Kaschel, E. Kasper and J. Schulze (2013). Direct bandgap narrowing in Ge LED's on Si substrates, *Opt. Express*, **21**(2), 2206–2211.

19. J. Michel, J. Liu and L. C. Kimerling (2010). High-performance Ge-on-Si photodetectors, *Nat. Photonics*, **4**, 527–533.

20. E. Kasper, M. Kittler, M. Oehme and T. Arguirov (2013). Germanium tin: silicon photonics toward the mid-infrared, *Photonics Res.*, **1**(2), 69–76.

21. E. Kasper (2016). Group IV heteroepitaxy on silicon for photonics, *J. Mater. Res.*, **31**, 3639–3648.

22. T. S. Perova, E. Kasper, M. Oehme, S. Cherevkov and J. Schulze (2017). Features of polarized Raman spectra for homogeneous and non-homogeneous compressively strained GeSn alloys, *J. Raman Spectrosc.*, **48**, 993–1001.

23. L. Kormos, M. Kratzer, K. Kostecki, M. Oehme, T. Sikola, E. Kasper, J. Schulze and C. Teichert (2017). Surface analysis of epitaxially grown GeSn alloys with Sn contents between 15% and 18%, *Surf. Interface Anal.*, **49**, 297–302.

24. B. Schwartz, P. Saring, T. Arguirov, M. Oehme, E. Kasper, J. Schulze and M. Kittler (2016). Analysis of EL emitted by LEDs on Si substrates

containing GeSn/Ge multi quantum wells as active layers, *Solid State Phenom.*, **242**, 361–367.

25. N. von den Driesch, et al. (2018). Advanced GeSn/SiGeSn group IV heterostructure lasers, *Adv. Sci.*, **5**, 1700955.
26. V. A. Timofeev, A. I. Nikiforov, A. R. Tuktamyshev, V. I. Mashanov, I. D. Loshkarev, A. A. Bloshkin and A. K. Gutakovskii (2018). Pseudomorphic GeSiSn, SiSn and Ge layers in strained heterostructures, *Nanotechnology*, **29**, 154002.
27. W. Dou, M. Benamara, A. Mosleh, J. Margetis, P. Grant, Y. Zhou, S. Al-Kabi, W. Du, J. Tolle, B. Li, M. Mortazavi and S.-Q. Yu (2018). Investigation of GeSn strain relaxation and spontaneous composition gradient for low - defect and high-Sn alloy growth, *Sci. Rep.*, **8**, 5640.